Kovove Mater. 62 2024 119–128
DOI: 10.31577/km.2024.2.119

Diffusion behavior of Cr and V elements in the 50CrVA steel under high-temperature oxidation and surface treatment processes

Peng Peng[1], Peng Zhang[2], Yueqiang Yang[3], Chunmei Yang[4], Sensen Chai[1], Qingwei Dai[1]*

[1] *School of Metallurgy and Material Engineering, Chongqing University of Science and Technology, Chongqing 401331, P. R. China*
[2] *Guangdong Guangqing Metal Technology Co., Ltd, Guangdong, P. R. China*
[3] *Daye Special Steel Co., Ltd, Hubei, P. R. China*
[4] *CISDI Engineering Technology Co., Ltd, Chongqing, P. R. China*

Received 8 November 2022, received in revised form 21 January 2024, accepted 9 May 2024

Abstract

This work investigates the diffusion behavior of Cr and V elements in 50CrVA steel under heating at 950 °C for 30 min, followed by shot peening treatment. The results show that the 50CrVA steel is significantly oxidated. The oxides are mainly Fe_2O_3, Fe_3O_4, and $FeCr_2O_4$. The Cr element is enriched at the transition layer between the oxides and the matrix. The V element is homogeneously distributed in the oxidation layer and Fe matrix. After the shot peening treatment, the oxides are successfully removed. The oxides containing the V element form during the shot peening treatment. The oxides strengthen surfaces but lead to uneven surfaces. The relatively low heating temperature can effectively decrease the thickness of the oxide layer and reduce V oxides formed in the shot peening process, which is conducive to improving the surface quality.

K e y w o r d s: 50CrVA steel, oxidation, surface quality

1. Introduction

Leaf springs are elastic components in automobile suspension systems, requiring good reliability, simple structure, and low cost [1–3]. As an essential part of the automobile, the reliability of leaf spring performance and quality directly affects its driving safety. Furthermore, leaf springs are subjected to great alternating loads during driving [4–6]. Therefore, automobile manufacturers have high requirements for the high surface quality of the leaf springs.

The 50CrVA steel is a medium carbon alloy spring steel with a specific strength and good plasticity [7, 8]. It is widely used to manufacture automobile leaf springs [9]. High-temperature treatment is usually adopted for 50CrVA steel to ensure high mechanical performance. However, the high-temperature treatment generates oxides, which damage the surface quality [10]. Although the shot peening treatment removes the surface oxide layer, the surface quality is still not optimistic. The formation of oxides has an important effect on surface quality. The various alloying elements play different roles in the oxidation process, which hinders or promotes the oxidation process [11]. Therefore, understanding the diffusion behavior of the alloying elements in the 50CrVA steel under high-temperature oxidation and shot peening treatment processes is very important to control the surface quality.

For the 50CrVA steel, the Cr and V elements are the main alloying elements. Previous studies [12–14] show that Fe-Cr steel can form a continuous Cr enrichment layer between the matrix and iron oxide at high temperatures. Cr and V carbide composite coatings are reported to improve the corrosion resistance and wear resistance of the steel [15, 16]. Li et al. [17] discovered the chromium delamination phenomenon of T92 high chromium alloy steel under high-temperature conditions. In addition, the formation of oxides is affected by the amount of Cr added to the Fe-base alloy [18, 19]. When the Cr content reaches 5 %, the Fe oxides react with the Cr element in the FeO phase region to form $FeCr_2O_4$, and the solubil-

*Corresponding author: e-mail address: daiqingwei@cqust.edu.cn

Table 1. The main chemical compositions of the 50CrVA steel (wt.%)

C	Si	Mn	P	S	Ni	V	Cr
0.346	0.21	0.613	0.019	0.002	0.013	0.103	0.776

ity of the spinel structure can be suppressed due to its stability. Although the diffusion behavior of the Cr element has been widely investigated, the reports about the V element are still limited. Meanwhile, whether there are other effects of the two elements is also unknown.

In this work, the 50CrVA steel is selected as the object. The diffusion behavior of Cr and V elements under heating at 950 ℃ for 30 min, followed by shot peening treatment, is investigated. Meanwhile, the formation of oxides and their effects during heating and surface treatment are discussed in detail.

2. Experimental procedures

The commercial 50CrVA steel was purchased from Baowu Steel in China. The related chemical compositions are displayed in Table 1. The samples for oxidation were polished with SiC paper to mirror the surface. The oxidation process was performed in the ordinary resistance furnace (KJ-V1200-12LW). The heating rate was 20 ℃ min^{-1}. When the temperature was raised to 950 ℃, the samples were put into the furnace and heated for 30 min. The cooling process was air cooling. The contrast sample was protected by argon in a hypoxic environment. The shot peening process was adopted to remove the oxide from the surface. The holding time of the shot peening was 30 min. The diameter of the steel shot was 5 mm, and the shot peening pressure was 0.5 MPa.

The microstructure and the element distribution were observed by optical microscopy (OM, MDS400), X-ray diffraction (XRD, Rigaku Ultma IV), scanning electron microscopy (SEM, JEOL 7800F), and energy-dispersive X-ray spectroscopy (EDS). The EDS line analysis and mapping analysis were adopted to identify the chemical composition of the oxides. The samples were cut by an electric spark and polished to mirror to obtain a high-quality cross-section. Samples for OM, XRD, and SEM observation were polished with the SiC paper (200#–4000#) to make the viewing surface mirror. OM samples were eroded by 4 % alcohol nitrate. XRD test parameters: tube voltage 40 kV, tube current 200 μA, Cu target, diffraction width DS = SS = 1°, RS = 0.3 mm, scanning speed 2.000 (d min^{-1}), scanning range 25°–85°. SEM test parameters: accelerating voltage 15 kV, probe current 8 nA, working distance 10 mm.

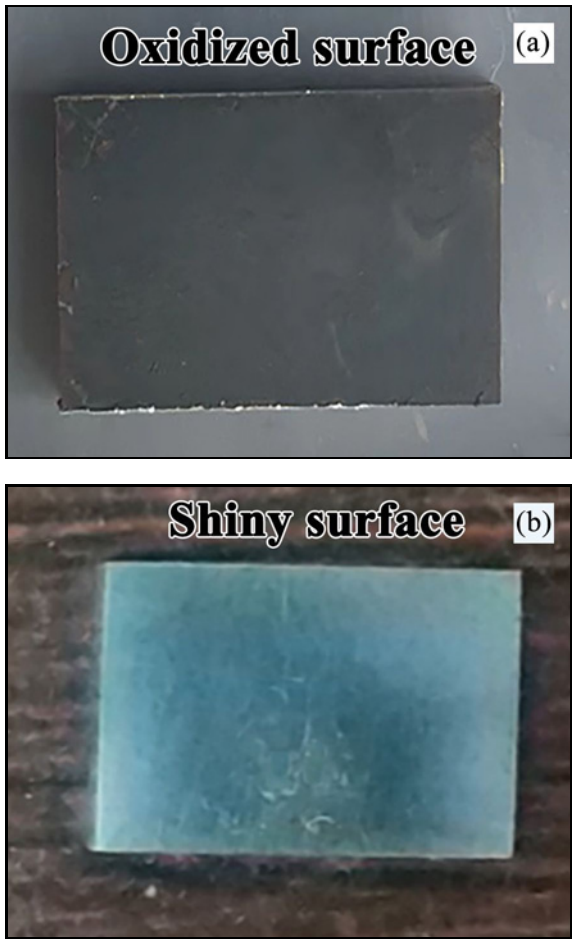

Fig. 1. The macro surface of the 50CrVA steel after heating at 950 ℃ for 30 min in an ordinary resistance furnace: (a) heating in the air and (b) heating in the hypoxic environment.

3. Results

3.1. High-temperature heating process

Figure 1 shows the macro surface of the 50CrVA steel after heating at 950 ℃ for 30 min in an ordinary resistance furnace. As shown in Fig. 1a, the sample surface is significantly oxidized under heat treatment in the air. As a result, the surface exhibits a bumpy state and is partially green. In comparison, the sample heating in the hypoxic environment remains almost flat and shiny. Therefore, the 50CrVA steel oxidates in the oxygen-containing environment.

To identify the composition of the oxide in the 50CrVA steel, the XRD, SEM, and EDS point analyses were employed. The results are shown in Fig. 2. Fe_3O_4 and Fe_2O_3 can be identified according to the XRD pattern. Since the diffraction peaks of the Fe_3O_4 and $FeCr_2O_4$ phases overlap, the $FeCr_2O_4$ phase is uncertain. The SEM image shows three layers: the oxidation layer, the transition layer, and the matrix. The

Table 2. EDS point analysis results

Elements	Spectrum number							
	1	2	3	4	5	6	7	8
Fe	42.2	41	60.7	58	64.1	88.6	88.4	81.4
O	33.6	31.4	31.6	31.1	30.2	0.2	0.3	6.3
Cr	12.4	12.7	1.3	1.8	0.1	0.9	0.9	1.7
C	5.1	9.6	5.6	8.1	5	9	9.5	9.3
Si	4.4	2.9	0.2	0.4	0	0.3	0.2	0.4
V	1.8	2	0.1	0.3	0	0.1	0.1	0.2
Mn	0.6	0.4	0.5	0.4	0.5	0.8	0.6	0.6

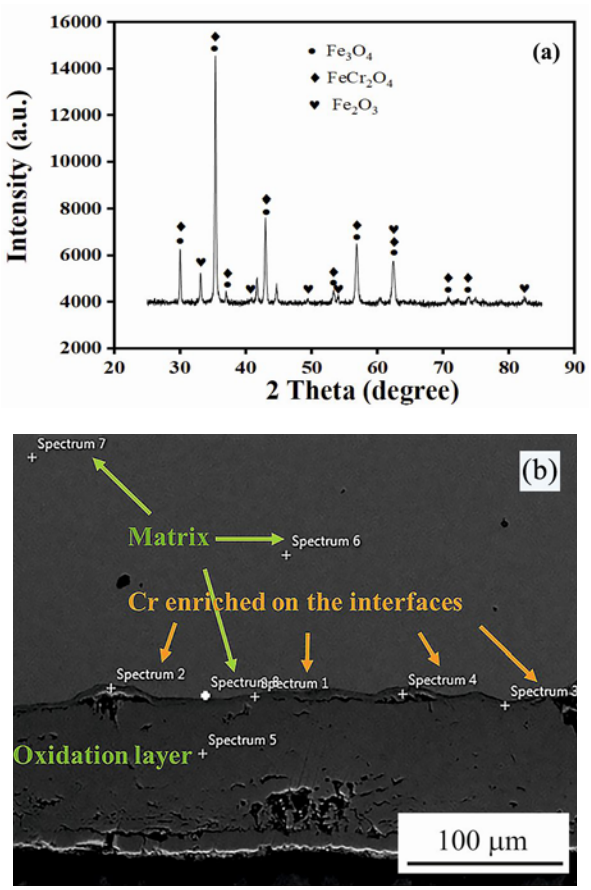

Fig. 2. XRD pattern, SEM, and related EDS point analysis results of the oxidized interface, (a) XRD pattern, and (b) SEM image.

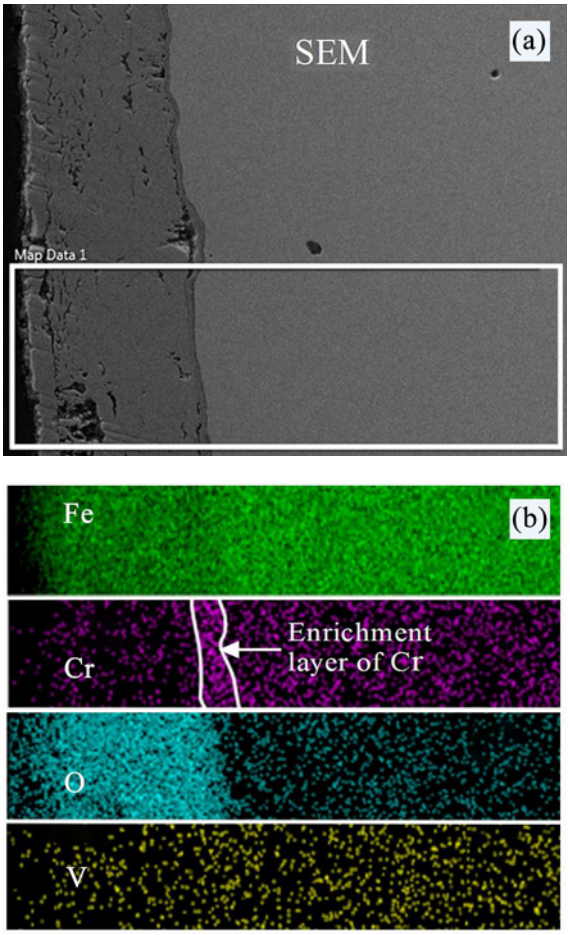

Fig. 3. EDS mapping analysis results of the oxidized interface.

EDS results are displayed in Table 2. Spectrum 5 illustrates that the oxide layer is mainly an iron oxide compound. According to the literature reported [20], the iron oxide compound may be Fe_3O_4. In addition, the oxidation layer exhibits a relatively compact state. It is worth noting that the Cr and V elements are enriched at the interface between the oxidation layer and matrix, as shown by the spectra 1–4. This illustrates that the diffusion of the Cr atoms differs from that of the matrix Fe atom during the high-temperature oxidation process.

Figure 3 shows the EDS mapping results of the oxidation layer of the 50CrVA steel. The oxidation layer mainly contains Fe and O elements. The Cr element is enriched at the transition layer. The V element is homogeneously distributed in the oxidation

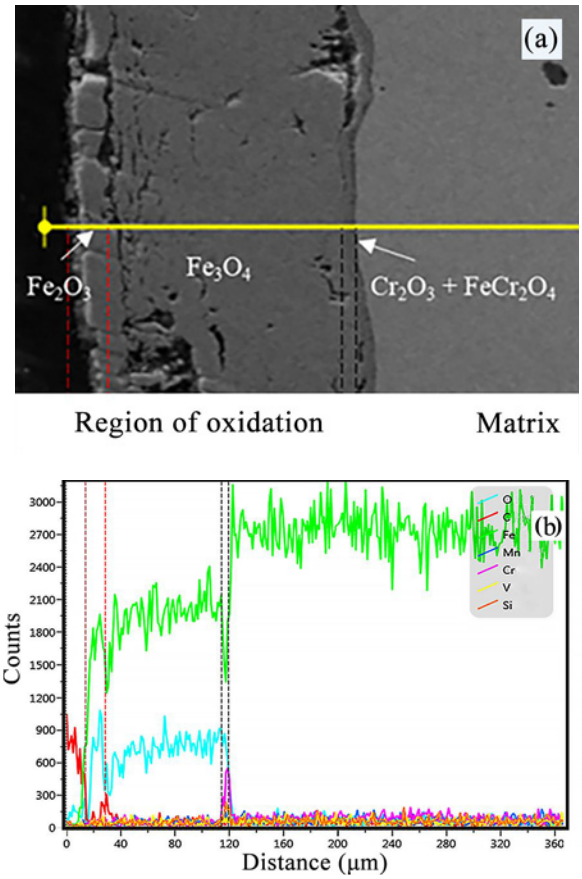

Fig. 4. EDS line analysis results of the oxidized interface.

layer and Fe matrix. Combined with the XRD results, the Cr-containing second phase can be considered the $FeCr_2O_4$ phase.

To further evaluate the layer thickness and elemental composition, the EDS line analysis results are shown in Fig. 4. The thickness of the oxidation layer is about 95 μm. The thickness of the Cr-enriched transition layer is about 8 μm. In addition, the oxidation layer is divided into two parts, containing outer and inner layers. According to EDS line analysis results, the thickness of the outer layer is about 15 μm, while that of the inner layer is about 80 μm. Meanwhile, the oxygen content of the outer layer is higher than that of the inner layer. Therefore, it can be identified that the outer layer is Fe_2O_3, and the inner layer is Fe_3O_4.

3.2. Shot peening treatment

The shot peening treatment is generally used to remove the oxidation layer. After 30 minutes of shot peening, the oxidation layer of the 50CrVA steel is almost removed, as shown in Fig. 5. However, the bumpy regions of the surface are still preserved. Compared with the sample before peening, the surface is relatively smoother. Only part of the hollow and bulge zones remains, as shown in Fig. 5.

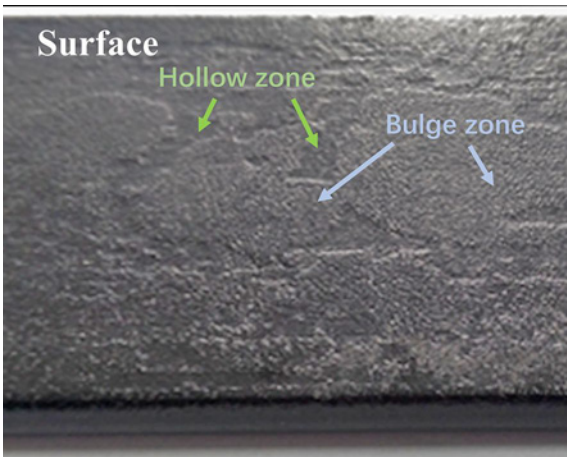

Fig. 5. The macro surface of the 50CrVA steel after shot peening treatment.

Figure 6 displays the OM microstructure of the 50CrVA steel after the shot peening treatment. The interior matrix exhibits a uniform microstructure (Fig. 6a). However, the interface shows two typical structures containing a bulge and a hollow zone, as shown in Fig. 6b. Further magnified images of the two zones are shown in Figs. 6c,d. Again, some coarse white particles can be observed. In addition, the microstructure of the hollow zone exhibits a fine structure, with only a small fraction of these coarse particles. Such variation presents that the decarburization phenomenon has occurred in the bulge zone.

Figure 7 shows the element distribution of the bulge zone in the 50CrVA steel after the shot peening treatment. From the SEM result, some holes and metal carbides can be observed. EDS mapping illustrates that particles in the holes are enriched with V and O elements, which can be considered vanadium oxides. The occurrence of vanadium oxides in the bulge zone illustrates that the vanadium oxides provide good strength to avoid being shot down during shot peening treatment.

Figure 8 shows the element distribution of the hollow zone in the 50CrVA steel after the shot peening treatment. From the SEM results, the hollow zone is relatively flat and has no holes. The element distribution maps display that vanadium oxides occur on the surface. Meanwhile, these vanadium oxides show a specific direction, mainly related to the stress state during the shot peening treatment. The existence of the vanadium oxides indicates that they have some toughness and are not easily shot down during shot peening. Therefore, the hollow zone shows a certain level.

4. Discussion

The 50CrVA steel exhibits a significant oxidation

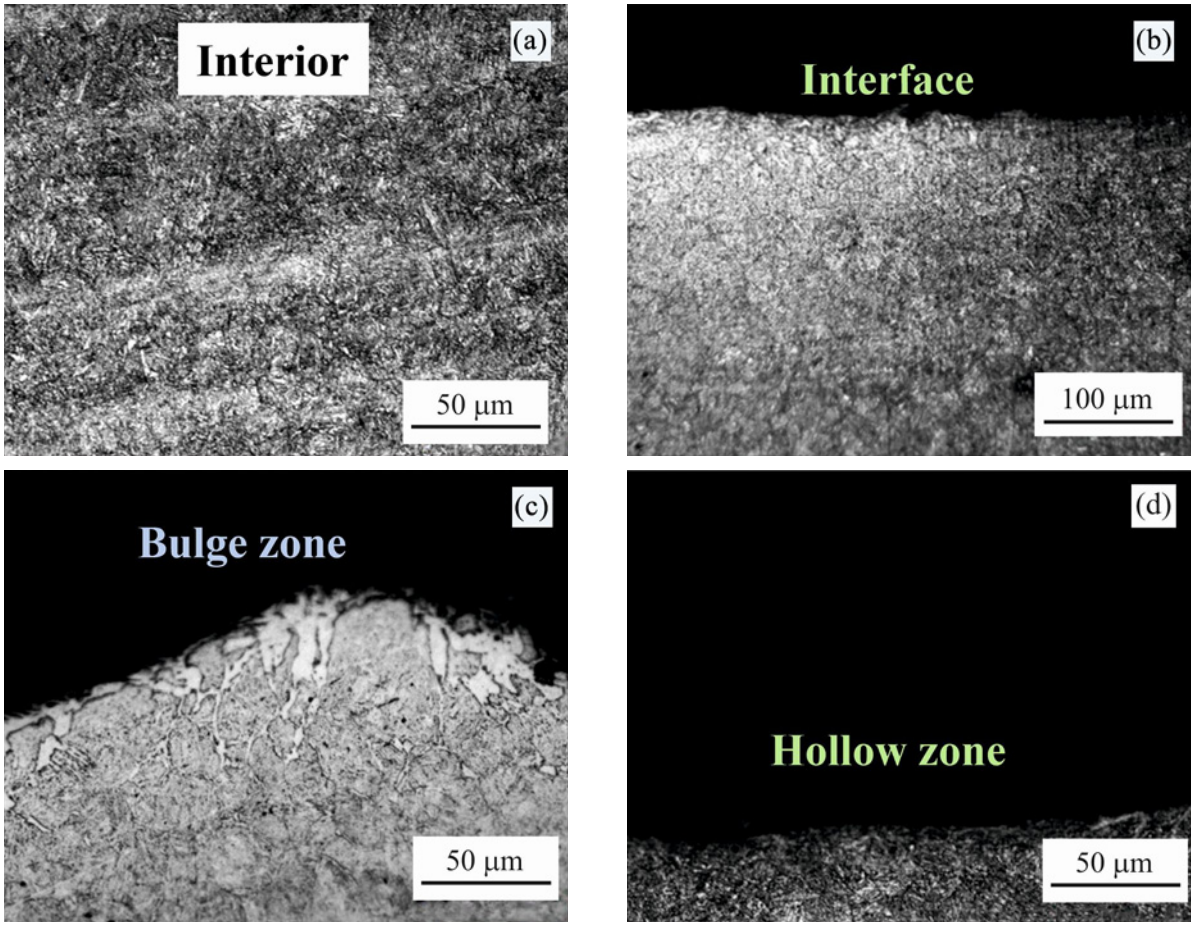

Fig. 6. OM images of the 50CrVA steel after shot peening treatment, (a) interior zone, (b) interface, (c) bulge zone, and (d) hollow zone.

reaction during the high-temperature heating process. Alloying elements of Cr and V play an important role in the oxidation reaction and following shot peening treatment. Elucidating the diffusion behavior of the alloying elements during the oxidation reaction is very important for further understanding the oxidation mechanism of 50CrVA steel.

The oxidation reaction of steel has been reported in the literature [21–23]. When the oxidation temperature is over 900 ℃, the partial oxygen pressure in the hot air is higher than the partial equilibrium pressure of oxides such as FeO, Fe_3O_4, and Fe_2O_3. Hence, the oxides can be nucleated. The partial oxygen pressure variation for the alloying elements can also promote metallic oxide formation. According to Ellingham's diagram [24], the degree of difficulty of their formation is in the following order: $Fe_2O_3 > Fe_3O_4 > FeO > Cr_2O_3$. Therefore, the oxidation reaction of the Cr-containing steel can be understood by the following reactions [25–27]:

$$Fe + O_2 \rightarrow 2FeO, \quad (1)$$

$$4Cr + 3O_2 \rightarrow 2Cr_2O_3, \quad (2)$$

$$FeO + Cr_2O_3 \rightarrow FeCr_2O_4, \quad (3)$$

$$6FeO + O_2 \rightarrow 2Fe_3O_4, \quad (4)$$

$$4Fe_3O_4 + O_2 \rightarrow 6Fe_2O_3. \quad (5)$$

In the initial stage, the reaction is dominated by the oxide formation of FeO and Cr_2O_3. As the reaction developed, the part of FeO reacted with Cr_2O_3 and formed $FeCr_2O_4$. The other FeO continues to react with oxygen and form Fe_3O_4. At the end of the oxidation reaction, the Fe_3O_4 further reacts with oxygen, forming Fe_2O_3. The above reaction process provides the opportunity for various oxides to nucleate. It is worth noting that the Cr element is involved in a reaction with an oxide in the reaction process. This process results in the diffusion of the Cr element. According to Li et al. [17], the diffusion behavior produces barren and enriched regions of the Cr element. Thus, after forming the Cr_2O_3, the newly formed FeO will react with the Cr_2O_3, forming $FeCr_2O_4$. The newly formed FeO generally exists between the matrix and the oxide. Therefore, the reaction between FeO and Cr_2O_3

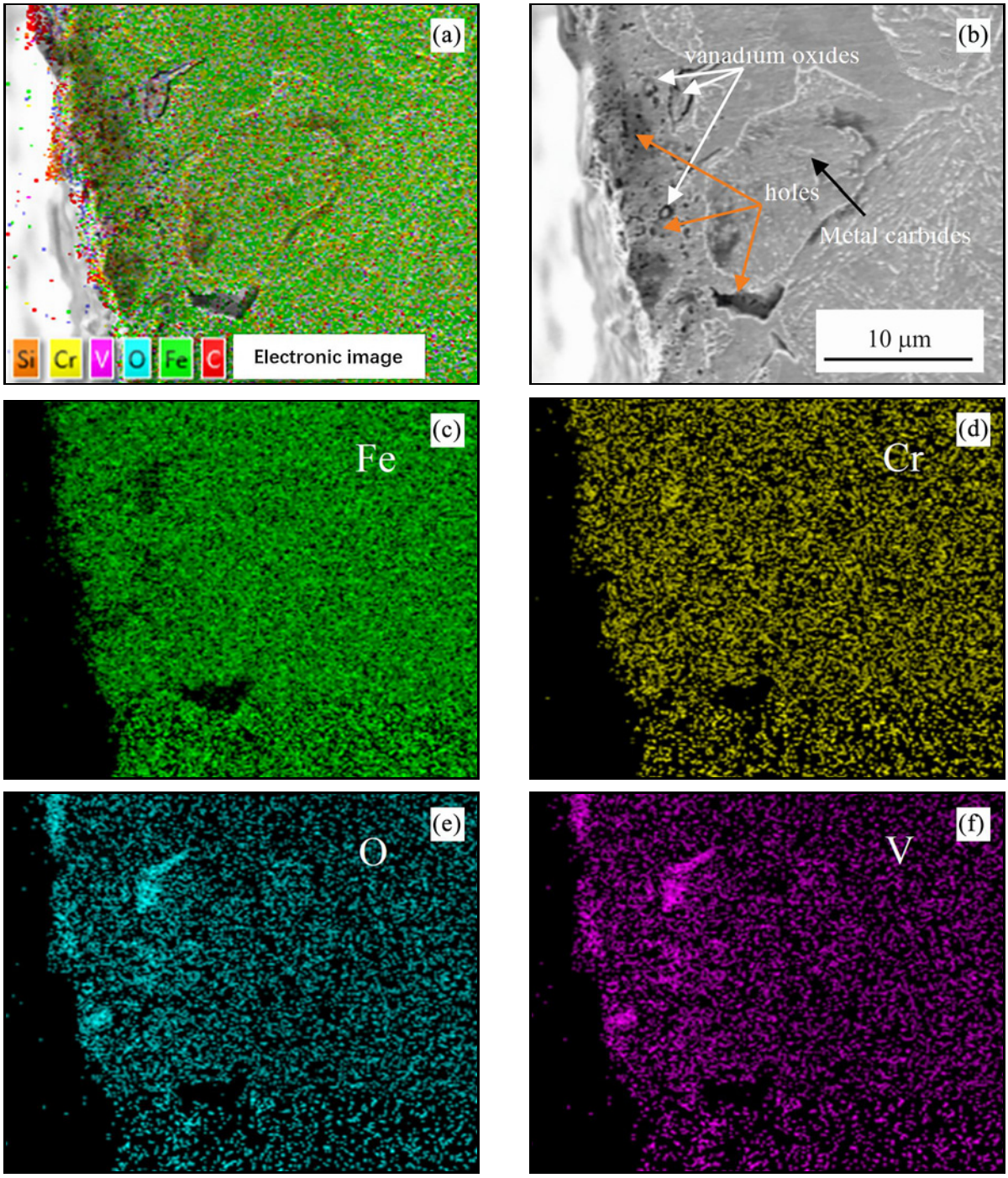

Fig. 7. EDS mapping analysis results of the bulge zone after shot peening treatment.

results in a Cr-rich region appearing at the interface between the oxide and the matrix.

The Cr-rich region is beneficial in hindering the further progress of the oxidation reaction. Hao et al. [20] reported that the activation energies of Fe-1Cr-0.2Si and F-0.2Si steels were calculated to be 217.785 and 215.095 kJ mol^{-1}, respectively. This illustrates that adding the Cr element increases the activation energy, thus slowing down the oxidation reaction. According to Arrhenius, the relationship between activation energy and oxidation rate constant of the steel can be understood by the following Eq. (6) [20]:

$$K_{\mathrm{p}} = K_0 \exp\left(-Q/RT\right), \tag{6}$$

where K_{p} is the oxidation rate constant, K_0 is the model constant, Q is the activation energy, R is the gas constant, and T is the oxidation temperature. Taking the logarithm, Eq. (6) can be written as:

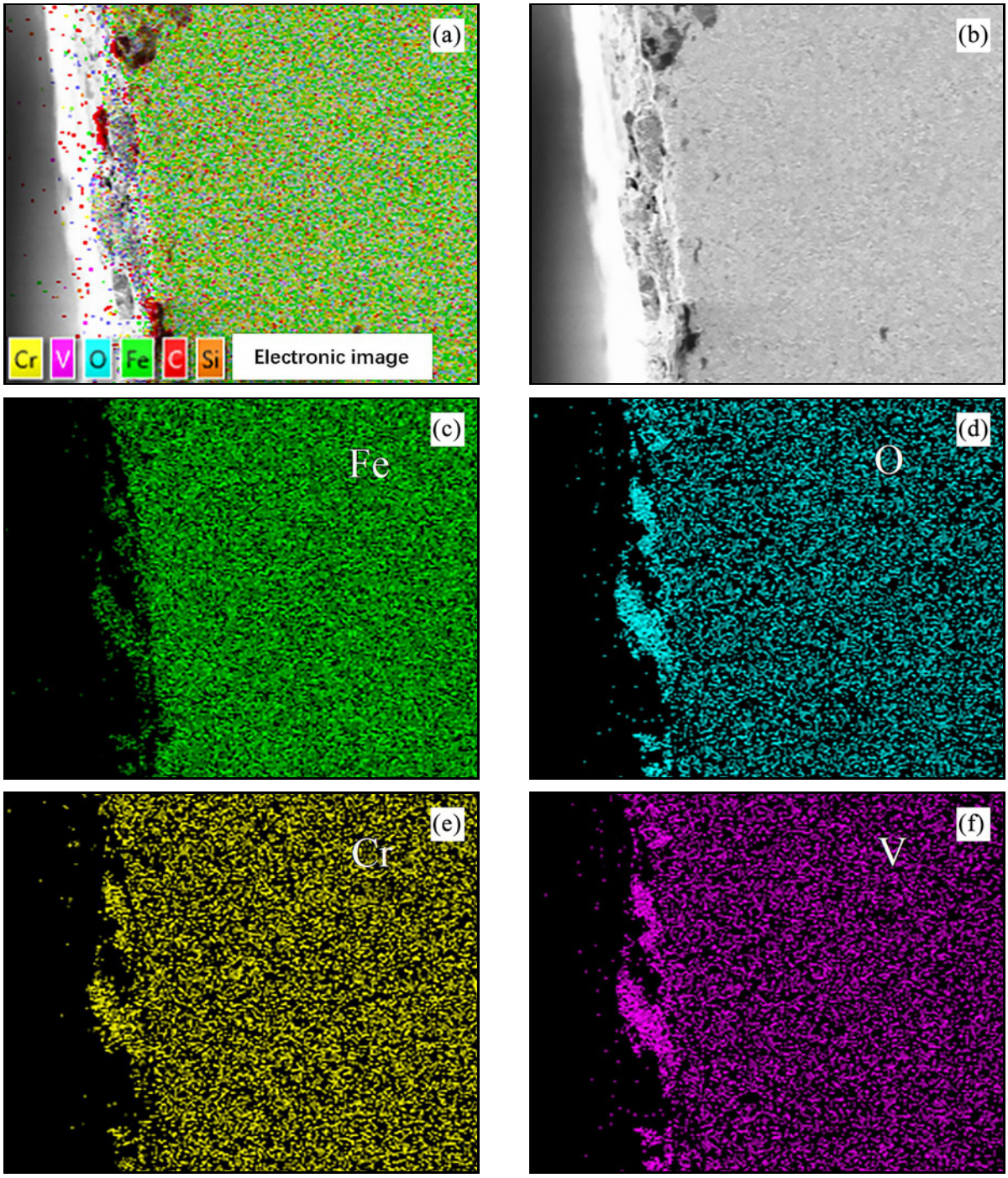

Fig. 8. EDS mapping analysis results of the hollow zone after shot peening treatment.

$$\ln K_{\mathrm{p}} = \ln K_0 - Q/RT. \tag{7}$$

The key factors influencing the oxidation behavior are K_{p}, K_0, Q, R, and T. The oxidation rate constant is closely related to the activation energy and the oxidation temperature. The activation energy increases with the addition of the Cr element. For 50CrVA steel, the oxidation temperature is the most crucial parameter. Increasing the oxidation temperature is beneficial to the formation of the oxidation. According to Balaško et al. [28], when the tool steel is oxidated at 400 and 700 ℃, the thickness of the oxidation layer is increased from 3.3 μm to 223.6 μm.

In order to clarify the effects of the oxidation temperature on the 50CrVA steel, the steel is oxidated at 1000 ℃ for 30 min. The related cross-section microstructure and the EDS line analysis result are displayed in Fig. 9. The thickness of the oxidation layer reached 192 μm, which is higher than that of the sample heated under 950 ℃ (95 μm). The outside layer

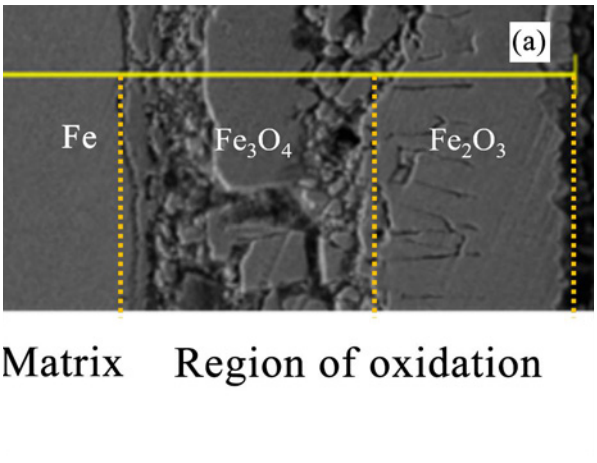

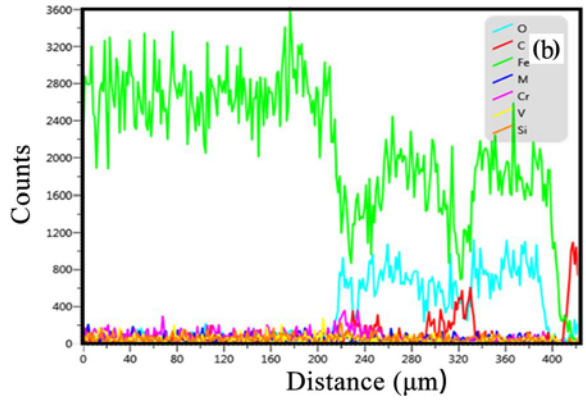

Fig. 9. EDS line analysis results of the oxidized interface in the 50CrVA steel after heating at 1000 °C for 30 min.

is the Fe_2O_3, while the inner layer is the Fe_3O_4. In addition, the Cr forms a continuous enrichment layer on the surface, which can protect the matrix. However, this protective effect is feeble under temperatures higher than 950 °C. Therefore, with the increment of the oxidation temperature, the oxidation reaction is rapidly intensified, and an oxide containing the Cr element is difficult to hinder the oxidation reaction.

An interesting phenomenon was found after shot peening to remove the oxide layer on the surface. Oxides containing V element appear in both the bulge and hollow zones. The difference between the two zones is that the oxides are in different regions. Oxides in the bulge zone are located in the matrix, while the oxides in the hollow zone are on the surface. Notably, the oxides containing the V element are only observed in the sample after the shot peening treatment. After high-temperature oxidation, the V element is uniformly distributed in the matrix, as shown in Fig. 3. This illustrates that oxygen enters the matrix and reacts with the V element when the steel shot removes the oxide layer from the surface. The formation of the oxides containing the V element generates the second phase strengthening effect, which can resist the impact of steel shot. The oxides protect the matrix in the bulge zone to avoid further shedding. The oxides are bombarded off the surface in the hollow zone, forming a layered structure.

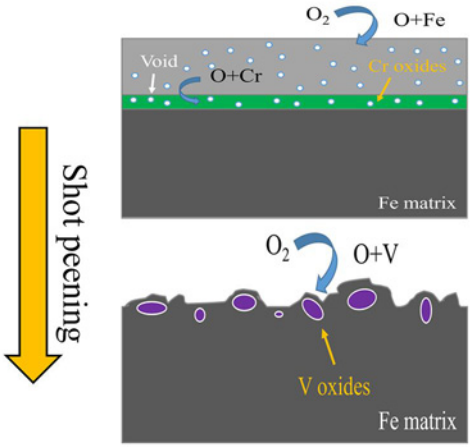

Fig. 10. Schematic diagram of Cr and V elements diffusion behavior in the 50CrVA steel under high-temperature oxidation and surface treatment process.

To sum up, the reaction of the Cr and V elements during the oxidation process and the shot peening treatment can be understood in Fig. 10. Under the high-temperature oxidation process, Fe atoms react with O atoms and form oxides containing Fe. The Cr element in the steel also combines with the O atoms and forms Cr oxides. These oxides prevent oxygen atoms from further interacting with Fe atoms. Meanwhile, these oxides are loose and have microvoids in them. After the shot peening, the oxides are successfully removed. However, oxides containing the V element form during the shot peening treatment. These oxides containing V elements can strengthen surfaces but can also lead to uneven surfaces. It is worth noting that the V element enriched region is found on the surface after heating at 1000 °C for 30 min (Fig. 9). It can be predicted that after heating at 1000 °C, the surface of the steel will be more uneven after shot peening, which is consistent with the actual production results. With the increase in heating temperature, the surface smoothness will become worse. Therefore, in a certain temperature range, reducing the heat treatment temperature can effectively decrease the thickness of the oxide layer and reduce the V oxides formed in the shot peening process, which is conducive to improving the surface quality.

5. Conclusions

This work investigates the diffusion behavior of Cr and V elements in 50CrVA steel under high--temperature oxidation and surface treatment. The

main findings are displayed as follows:

(1) After heating at 950 °C for 30 min, the 50CrVA steel is significantly oxidated. The oxides are mainly Fe_2O_3, Fe_3O_4, and $FeCr_2O_4$. The Cr element is enriched at the transition layer. The V element is homogeneously distributed in the oxidation layer and Fe matrix.

(2) The oxides are successfully removed after the shot peening treatment. Oxides containing V element form during the shot peening treatment. The oxides can strengthen surfaces but can also lead to uneven surfaces. Heating at high temperatures will generate a V-enriched region, easily decreasing the surface quality.

(3) Enriching the Cr element protects the matrix from further oxidation. However, enriching the V element will damage the surface quality by forming the oxides containing the V element during the shot peening treatment.

(4) Choosing a relatively low heating temperature can effectively decrease the thickness of the oxide layer and reduce the V oxides formed in the shot peening process, which is conducive to improving the surface quality. The findings can provide theoretical support for the engineering application of heat treatment for 50CrVA steel.

Acknowledgements

This work is supported by the Innovation Research Group of Universities in Chongqing (CXQT21030), Chongqing Talents: Exceptional Young Talents Project (CQYC201905100), and Chongqing Youth Expert Studio. Peng Peng and Zhang Peng contributed equally to this work.

References

[1] V. Khatkar, B. K. Behera, R. N. Manjunath, Textile structural composites for automotive leaf spring application, Composites B 182 (2020) 182107662. https://doi.org/10.1016/j.compositesb.2019.107662

[2] V. Khatkar, B. K. Behera, Experimental investigation of textile structure reinforced composite leaf spring for their cyclic flexural and creep behaviour, Compos. Struct. 258 (2021) 113439. https://doi.org/10.1016/j.compstruct.2020.113439

[3] X. Zou, B. Zhang, G. Yin, Analysis of stiffness and damping performance of the composite leaf spring, Sci. Rep. 12 (2022) 6842. https://doi.org/10.1038/s41598-022-11055-5

[4] T. G. Loganathan, K. Vinoth Kumar, S. Madhu, Flexural and fatigue of a composite leaf spring using finite element analysis, Mater. Today: Proc. 22 (2020) 1014–1019. https://doi.org/10.1016/j.matpr.2019.11.265

[5] A. Atig, R. Ben Sghaier, R. Seddik, R. Fathallah, A simple analytical bending stress model of parabolic leaf spring, P. I. Mech. Eng. C-J. Mech. 232 (2017) 1838–1850. https://doi.org/10.1177/0954406217709302

[6] A. Atig, R. Ben Sghaier, R. Seddik, R. Fathallah, Reliability-based high cycle fatigue design approach of parabolic leaf spring, P. I. Mech. Eng. C-J. Mda. 233 (2017) 588–602. https://doi.org/10.1177/1464420716680499

[7] Y. Wang, L. Fu, M. Zhou, Z. Zhou, X. Pang, S. Zhong, A. A. Volinsky, Thermodynamics analysis of multiple microelements' coupling behavior in high fatigue resistance 50CrVA spring steel with nanoparticles, Materials 12 (2019) 2952. https://doi.org/10.3390/ma12182952

[8] X.-P. Zhou, R.-S. Deng, J.-Y. Zhu, Three-layer-stacked pressure sensor with a liquid metal-embedded elastomer, J. Micromech. Microeng. 28 (2018) 085020. https://doi.org/10.1088/1361-6439/aac13c

[9] W. Xin, Q. Meng, J. Zhang, Y. Liang, Y. Jiang, Y. Deng, Z. Cheng, Effect of arsenic on the high temperature oxidation and hot shortness behaviour of copper-bearing steel, Metall. Res. Technol. 119 (2022) 313. https://doi.org/10.1051/metal/2022034

[10] H. H. Alsalla, C. Smith, L. Hao, Effect of build orientation on the surface quality, microstructure and mechanical properties of selective laser melting 316L stainless steel, Rapid Prototyping J. 24 (2018) 9–17. https://doi.org/10.1108/RPJ-04-2016-0068

[11] L. Zhu, P. Xue, Q. Lan, G. Meng, Y. Ren, Z. Yang, P. Xu, Z. Liu, Recent research and development status of laser cladding: A review, Opt. Laser Technol. 138 (2021) 106915. https://doi.org/10.1016/j.optlastec.2021.106915

[12] C. Juricic, H. Pinto, D. Cardinali, M. Klaus, C. Genzel, A. R. Pyzalla, Evolution of microstructure and internal stresses in multi-phase oxide scales grown on (110) surfaces of iron single crystals at 650 °C, Oxid. Met. 73 (2010) 115–138. https://doi.org/10.1007/s11085-009-9166-x

[13] G. D. West, S. Birosca, R. L. Higginson, Phase determination and microstructure of oxide scales formed on steel at high temperature, J. Microsc. 217 (2005) 122–129. https://doi.org/10.1111/j.1365-2818.2005.01409.x

[14] R. Y. Chen, W. Y. D. Yuen, Oxide-scale structures formed on commercial hot-rolled steel strip and their formation mechanisms, Oxid. Met. 56 (2001) 89–118. https://doi.org/10.1023/A:1010395419981

[15] A. Günen, E. Kanca, M. S. Karakaş, M. S. Gök, M. Kalkandelen, B. Kurt, M. Çetin, I. H. Karahan, Effect of thermal degradation on the properties and wear behavior of Cr-V-C composite coatings grown on ductile iron, Surface and Coatings Technology 419 (2021) 127305. https://doi.org/10.1016/j.surfcoat.2021.127305

[16] A. Günen, M. Kalkandelen, İ. H. Karahan, B. Kurt, E. Kanca, M. S. Gök, M. Serdar Karakaş, Properties and corrosion behavior of chromium and vanadium carbide composite coatings produced on ductile cast iron by thermoreactive diffusion technique, Journal of Engineering Materials and Technology 142 (2020) 041008. https://doi.org/10.1115/1.4047743

[17] K. Li, H. Ma, Y. He, J. Chang, S.-Y. Bae, K. Shin, Microstructural evolution and oxidation resistance of T92 boiler tube steel upon long-term supercritical

steam test, Fusion Eng. Des. 125 (2017) 361–366. https://doi.org/10.1016/j.fusengdes.2017.04.133
[18] C. Juricic, H. Pinto, D. Cardinali, M. Klaus, C. Genzel, A. R. Pyzalla, Effect of substrate grain size on the growth, texture and internal stresses of iron oxide scales forming at 450 °C, Oxid. Met. 73 (2010)15–41. https://doi.org/10.1007/s11085-009-9162-1
[19] A. I. Kahveci, G. E. Welsch, Oxidation of Fe-3 wt.% Cr alloy, Oxid. Met. 26 (1986) 213–230. https://doi.org/10.1007/BF00659185
[20] M. Hao, B. Sun, H. Wang, High-temperature oxidation behavior of Fe-1Cr-0.2Si steel, Materials 13 (2020) 509. https://doi.org/10.3390/ma13030509
[21] D. Zhang, Z.-M. Bi, H.-L. Sun, L. Cheng, Y.-X. Liu, Z.-Y. Hu, B. Wang, High-temperature oxidation mechanism of Fe-3.0wt.%Si electrical steel with hybrid atmosphere, J. Alloys Compd. 913 (2022) 165247. https://doi.org/10.1016/j.jallcom.2022.165247
[22] S. Zhang, Z. Jiang, H. Li, B. Zhang, P. Chang, J. Wu, H. Feng, H. Zhu, Catastrophic oxidation mechanism of hyper duplex stainless steel S32707 at high temperature in air, Mater. Charact. 145 (2018) 233–245. https://doi.org/10.1016/j.matchar.2018.08.041
[23] Y. Chen, X. Lou, L. Yang, C. Wang, K. Zhou, M. Chen, Q. Wang, S. Zhu, F. Wang, Oxidation and corrosion protection of ZG12Cr9Mo1Co1NiVNbNB (CB2) ferritic stainless steel by inorganic composite coatings at 650 °C, Corros. Sci. 177 (2020) 109000. https://doi.org/10.1016/j.corsci.2020.109000
[24] D. J. Young, High Temperature Oxidation and Corrosion of Metals, Elsevier 2008. ISBN: 978-0-08-100101-1
[25] Y. Chen, K. Sridharan, T. Allen, Corrosion behavior of ferritic-martensitic steel T91 in supercritical water, Corros. Sci. 48 (2006) 2843–2854. https://doi.org/10.1016/j.corsci.2005.08.021
[26] P. Ampornrat, G. S. Was, Oxidation of ferritic-martensitic alloys T91, HCM12A and HT-9 in supercritical water, J. Nucl. Mater. 371 (2007) 1–17. https://doi.org/10.1016/j.jnucmat.2007.05.023
[27] L. Tan, X. Ren, T. R. Allen, Corrosion behavior of 9–12% Cr ferritic-martensitic steels in supercritical water, Corros. Sci. 52 (2010) 1520–1528. https://doi.org/10.1016/j.corsci.2009.12.032
[28] T. Balaško, M. Vončina, J. Burja, B. Š. Batič, J. Medved, High-temperature oxidation behavior of tool steel with increased thermal conductivity, Oxid. Met. 98 (2022) 135–161. https://doi.org/10.1007/s11085-022-10119-1